Chemical Physics Impact 6 (2023) 100234

Contents lists available at ScienceDirect

Chemical Physics Impact

journal homepage: www.sciencedirect.com/journal/chemical-physics-impact

# Hexachlorobenzene (HCB) adsorption onto the surfaces of $C_{60}$, $C_{59}Si$, and $C_{59}Ge$: Insight from DFT, QTAIM, and NCI

Mohsen D. Mohammadi [a], Hewa Y. Abdullah [b,*], Hitler Louis [c], Emmanuel E. Etim [d], Henry O. Edet [c,*], Obinna C. Godfrey [e]

[a] School of Chemistry, College of Science, University of Tehran, Tehran 14176, Iran
[b] Physics Education Department, Faculty of Education, Tishk International University, Erbil, 44001, Kurdistan Region, Iraq
[c] Computational and Bio-Simulation Research Group, University of Calabar, Calabar, Nigeria
[d] Department of Chemical Sciences, Federal University Wukari, Wukari, Nigeria
[e] Department of Biochemistry, Faculty of Basic Medical Sciences, University of Calabar, Calabar, Nigeria

ARTICLE INFO

*Keywords:*
Hexachlorobenzene
Fullerene
Density functional theory
Adsorption

ABSTRACT

Several reports have shown that nanomaterials have been found to be effective for gas sensing application and the adsorption of hazardous organochloride. Herein, dispersion corrected density functionals; D3-B3LYP-D3, ωB97XD, M06-2X and PBE0 all at the 6-311G (d) basis set was used to study the interactions of metal-doped fullerenes (silicon ($C_{59}Si$) and germanium ($C_{59}Ge$)) with Hexachlorobenzene ($C_6C_{l6}$) gas molecule. The adsorption properties of the adsorbents viz; the pure fullerene nanocage ($C_{60}$) and the doped system; Silicon ($C_{59}Si$) and Germanium ($C_{59}Ge$) were all investigated in terms of reactivity, stability, bond order, intermolecular interaction, van der waals, and weak interaction as well as adsorption energy. The reactivity levels of the examined surfaces were observed within the same range at the B3LYP-D3/6-311G (d) level of theory to be 5.996 eV, 5.309 eV, and 5.188 eV for $C_{60,}$ $C_{59}Si$ and $C_{59}Ge$ adsorbents respectively. From our calculation for adsorption energies; the high negative value -1.010 eV of for the $C_{59}Ge$ nanocage suggests that the doped surface adsorbs hexachlorobenzene better in comparison to the other surfaces and adsorption is thermodynamically favored. The results for natural bond orbitals (NBO), quantum theory of atoms in molecules (QTAIM), and non-covalent interaction (NCI) were consistent across all systems and favored physical adsorption.

## 1. Introduction

Organochlorine (OC) pesticides are widely utilized across the world. They're chlorinated hydrocarbon derivatives with a variety of uses in the chemical and agricultural industries [1]. These compounds' extreme toxicity, slow disintegration, and bioaccumulation are well-known. Because of its high toxicity in the environment, bioaccumulation of HCB results in some level of toxicity [2]. Hexachlorobenzene gas (HCB), an organochloride with the chemical formula $C_6C_{l6}$, is very poisonous and insoluble in water. It's also flammable, but it takes a long time to ignite [3]. Hexachlorobenzene generates hazardous emissions of hydrochloric acid, carbon monoxide, and carbon dioxide when it decomposes [4]. It was previously used to treat seeds and control wheat [5]. In a number of processes, HCB is generated in trace amounts. Chemical waste, metal manufacture, and numerous combustion processes are all potential sources of HCB. Humans who are exposed to HCB risk having their immune and reproductive systems disrupted [6].

Many investigations have been undertaken to better understand the interaction between the adsorbing surface and the pollutant in order to develop gas sensing materials that can detect contaminated gasses [7]. The introduction of wave function analysis approaches has aided in anticipating the nature of intermolecular interactions even in large systems. Although there is no systematic classification of ab initio methods in the scholarly literature [8], Ahmed et al., studied the binding of HCB to a test set of molecules, which was developed to mimic representative functional groups of SOM and reported the dispersion effect from functionals used [9]. Wagner et al., studied the application of MOFs for the detection and adsorption of selected pesticides that are classified as POPs and reported high sensitivity of gas molecule [10]. The discovery of carbon-based nanoparticles paved the way for nanotechnology advancement in the field of inorganic nanomaterials [11].

Due to its features, including as heat resistance and

* Corresponding authors.
*E-mail addresses:* hewayaseen@gmail.com (H.Y. Abdullah), henryokonedet98@gmail.com (H.O. Edet).

https://doi.org/10.1016/j.chphi.2023.100234
Received 19 December 2022; Received in revised form 20 May 2023; Accepted 21 May 2023
Available online 24 May 2023

superconductivity, fullerene has been employed in gas adsorption experiments. Previous studies have found that doping the surface of fullerene improves its gas sensing and detection abilities. We investigated the adsorption behavior of hexachlorobenzene (HCB) gas molecules on the surface of fullerene ($C_{60}$) and doped fullerene nanocages made of silicon ($C_{59}Si$) and germanium ($C_{59}Ge$). B3LYP-D3, ωB97XD, M06-2X, and PBEO with 6-311G(d) basis set used to optimize the geometry of the isolated and adsorb surfaces, with the dispersion effect taken into account. The B3LYP-D3/6-311G(d) model of theory produced a stable surface in terms of electronic energy, which was then employed for wave function analysis. Quantum chemical descriptors were used to determine the reactivity and stability of surfaces in order to determine their adsorption properties. The natural bond orbital (NBO) was used to verify for bond order, charge delocalization, and stabilization energies. Quantum theory of atoms in molecules (QTAIM) and non-covalent interactions (NCI) were used to achieve intermolecular and van der waals interactions, which aid in understanding the adsorption behavior of gas molecules on surfaces. All of the studies were carried out in a vacuum.

## 2. Computational details

The hybrid-exchange correlation (PBE0 functional), meta hybrid GGA functional (M06-2X), the long-range dispersion correction functional by the Head-Gordon group (ωB97XD), and the Becke 3-parameter Lee–Yang–Parr functional with Grimme dispersion correction (B3LYP-D3) with the 6-311G (d) (split-valence triple-zeta) basis set in the Gaussian package were used to geometrically optimize nanocage and the adsorbate gas molecule [12–16]. The natural population analysis (NPA) from natural bond orbitals (NBO) was obtained using the NBO version 3.1 [17] embedded in the Gaussian software. Topology analysis using Baders theory for quantum theory of atoms-in-molecules (QTAIM) was conducted using the Multiwfn analyzer to study the intramolecular interactions between the fullerene and the pollutant [18,19]. Non-covalent interaction (NCI), which was also obtained utilizing the multiwfn analyzer with formated checkpoint files of optimal surface and gas molecule, was used to determine van der waals and hydrogen bond interactions [20]. The density of states diagrams was obtained using the GaussSum program [21]. Benchmark investigations show that the basis set utilized to simulate molecular orbitals is large enough [22]. The split valence basis set, on the other hand, affects the size of orbitals rather than their form [23]. The introduction of orbitals with angular momentum, which assist in showing the atom in the ground state, alleviates this constraint [23]. Wavefunction, stability, and frequency checks were examined in order to attain accuracy in calculations for zero-point energy corrections (ZPECs) [24]. The maximal force and displacement, as well as the convergence of the self-consistent field, were compared using threshold values (0.00045 Hartree/Bohr and 0.0018 Bohr) (SCF) [25]. Furthermore, during the calculations, the default convergence was not changed.

## 3. Result and discussion

### 3.1. Geometric analysis

To evaluate intermolecular forces, M06-2X, B3LYP-D3, ωB97XD, and PBE0 6-311G(d) were used to optimize selected surfaces in the investigation [12–16]. These functions are expected to calculate intermolecular interactions quickly and accurately. To evaluate their gas adsorbing characteristics, a nanocage ($C_{60}$) with a 1.45 Å bond length was chosen and doped with silicon and germanium. Doping is used to detect nanomaterial adsorption characteristics and patterns [26]. In the $C_{60}$ cage, a single atom of silicon or germanium replaced a carbon atom ($C_{59}Si$ & $C_{59}Ge$). The Doped nanocages in comparison with pure nanocage are displayed in Fig. 1. Electronic structure was altered due to slight changes in bond length which also resulted in difference in properties for doped nanocages. Aside increasing the interaction properties of

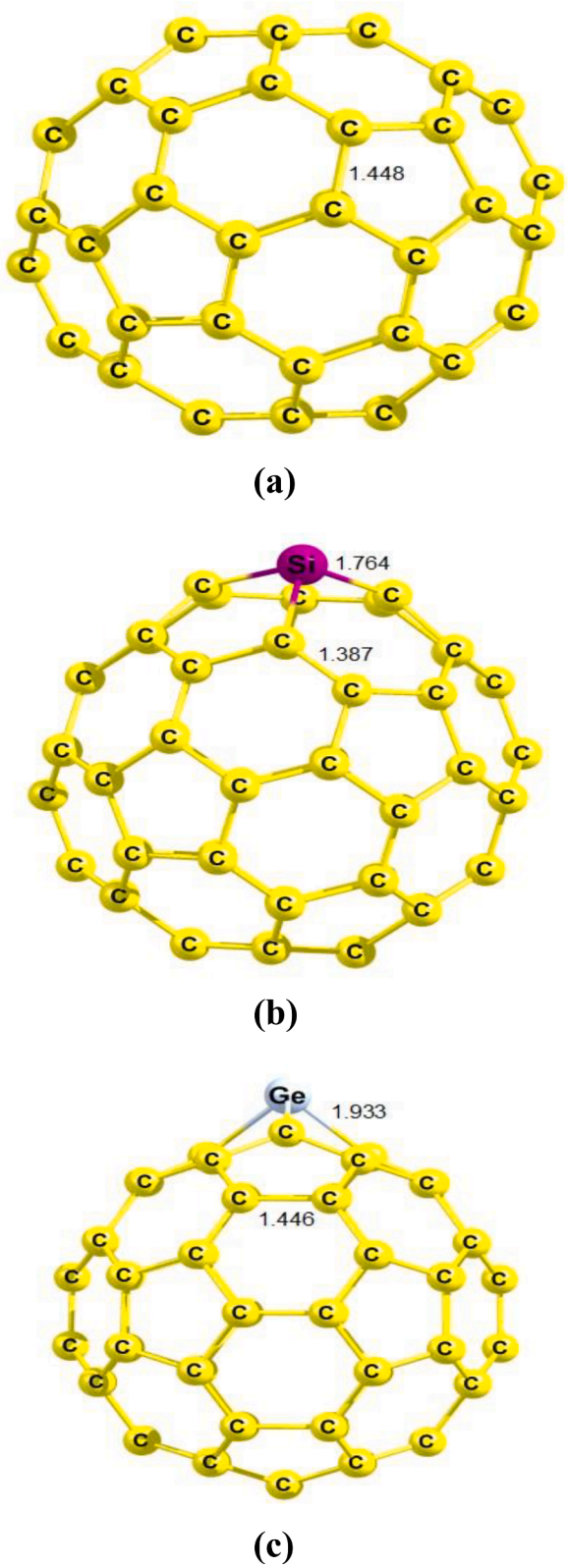


**Fig. 1.** Optimized surface using the B3LYP-D3/6-311G (d) level of theory for adsorption (a) $C_{60}$, (b) $C_{59}Si$, and (c) $C_{59}Ge$ showing bond length in Å.

adsorbent with gas molecule, the morphology of the dopants changed as well as HOMO, LUMO, and energy gap. To determine ZPEC (zero-point energy corrections) which must be added to the total energy, frequency calculations were performed [24]. As shown in Fig. 2, five possible sites for gas adsorption on the nanocage are presented by $S_1$, $S_2$, $S_3$, $S_4$ and $S_5$.

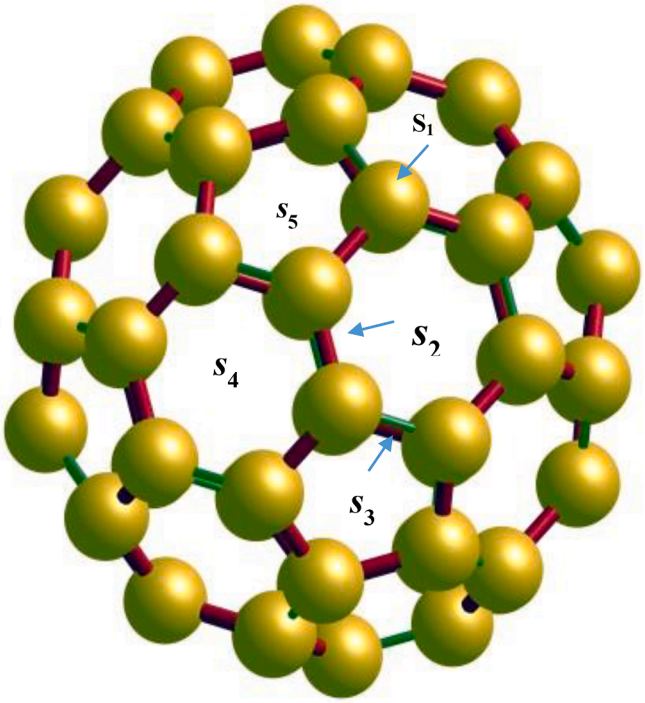


**Fig. 2.** Showing Possible Adsorption sites, ($S_1$), ($S_2$), ($S_3$), ($S_4$) ($S_5$) for the nanocage.

Structurally, Hexachlorobenzene molecule is symmetrical and can be placed on any of the five adsorption sites in different positions, angles and distances (Fig. 3). The approach used in this study involves attaching an atom from a gas molecule to the adsorbing surface at various angles and distances. As a result, a low-cost approach such as PM6 was employed [27]. To obtain the most energy-efficient construction, several orientations were chosen. To obtain a stable surface, optimization for the aforementioned functionals was repeated.

### 3.2. Frontier molecular orbital (FMO) analysis

The frontier molecular orbital describes the relationship between the highest occupied molecular orbital (HOMO) and the lowest unoccupied molecular orbital (LUMO). The reactivity, stability and conductivity of a molecule is determined by the energy gap in regards to other quantum descriptors; chemical potential, chemical hardness, and electrophilicity [28]. Molecules with low energy gap are said to be reactive whereas high values indicate stability. Calculated values for energy gap and quantum descriptors, using B3LYP-D3/6-311G (d) level of theory, are evident in Table 2. From the results comparable trend for energy gap was observed for the isolated cage and adsorb surface. For $C_{60}$ (5.996 to 4.983 eV), $C_{59}Si$ (5.309 to 4.029 eV) and $C_{59}Ge$ (5.188 to 4.427 eV) similar values observed is due to electronegative nature of atoms. The reactivity of a molecule is great when values for chemical hardness (η) are small. On adsorption of gas, values for chemical hardness decrease for $C_{60}$ (2.998–2.491), $C_{59}Si$ (2.654–2.014) & $C_{59}Ge$ (2.594–2.214). This is due to lower energy needed to move one electron from the HOMO to LUMO orbital. Electrophilicity index ($\omega$) shows the stabilization of a system [29]. A notable decrease in electrophilicity after adsorption of gasses by nanocage depicts stability and electron acceptor role of the molecule. $C_{59}Si$ with ($\omega$) index of 21.668 is more stable than $C_{60}$ 29.002 and $C_{59}Ge$ 29.386. upon adsorption. From the results similar trend for energy gap was observed for the isolated cage and adsorb surface [30]. From this result, the adsorption of Hexachlorobenzene gas reduces the energy gap of nanocages and improves its reactivity. So, charge density takes place upon adsorption. A visual image of HOMO, LUMO and energy level is shown in the density of state map and presented in Fig. 5. Calculations for quantum descriptors were done using this equation:

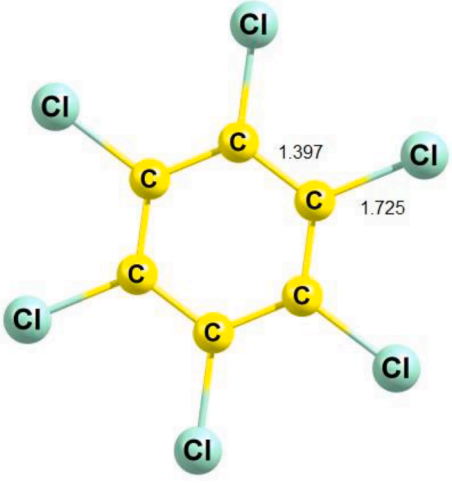


**Fig. 3.** Optimized gas molecule Hexachlorobenzene (HCB) using the B3LYP-D3/6-311G (d) level of theory showing bond length in Å.

$$EG = IP - EA \tag{1}$$

$$\eta = \frac{I - A}{2} \tag{2}$$

$$S = \frac{I}{2}\eta \tag{3}$$

$$\omega = \frac{\mu^2}{2}\eta \tag{4}$$

### 3.3. Adsorption energy

A large negative value for adsorption energy determines the stability and adsorption capabilities of an adsorbing surface [31]. Negative adsorption energy also suggests an exothermic process during gas molecule complexation on the adsorbing surface. Fig. 4 shows the most stable adsorption configuration of Hexachlorobenzene gas on $C_{60}$, $C_{59}Si$, and $C_{59}Ge$, as well as the contribution of dispersion correction. The B3LYP-D3/6-311G (d) level of theory was used to develop this relaxed adsorption configuration. Functionalized adsorption energy calculations were performed with PBE0, B97XD, M06-2X, and B3LYP-D3 at the /6-311G (d) level of theory in this study [12–16]. To calculate the adsorption energy ($E_{ads}$) of the gas molecules and nanocage this equation was utilized:

$$Eads = E_{surface/gas} - (E_{surface} + E_{gas}) \tag{5}$$

where $E_{surface/gas}$ is the energy of the adsorption of gas on surface and $E_{gas}$ and $E_{cage}$ are energies of the isolated gas and nanocage, respectively. Table 1 shows the calculated adsorption energies. For Hexachlorobenzene adsorption on $C_{59}Si$ and $C_{59}Ge$ surfaces, similar adsorption energy estimates have been reported for the ωB97XD, M06-2X, and B3LYP-D3 models of theory. However, the maximum value for HCB adsorption on $C_{60}$ was found in ωB97XD (−0.401 eV) and the lowest in PBE0 (−0.201 eV). In the case of HCB on $C_{59}Si$, the highest adsorption energy was still found in ωB97XD (−0.576 eV) and the lowest in PBE0 (−0.372 eV). The PBE0 results demonstrate how different the data would be if the dispersion effect was not taken into account. Using the B3LYP-D3, the adsorption of HCB on $C_{59}Ge$ was also found to have the greatest adsorption energy of −1.010 eV and the lowest of −0.569 eV in PBE0. High adsorption energies for ωB97XD and

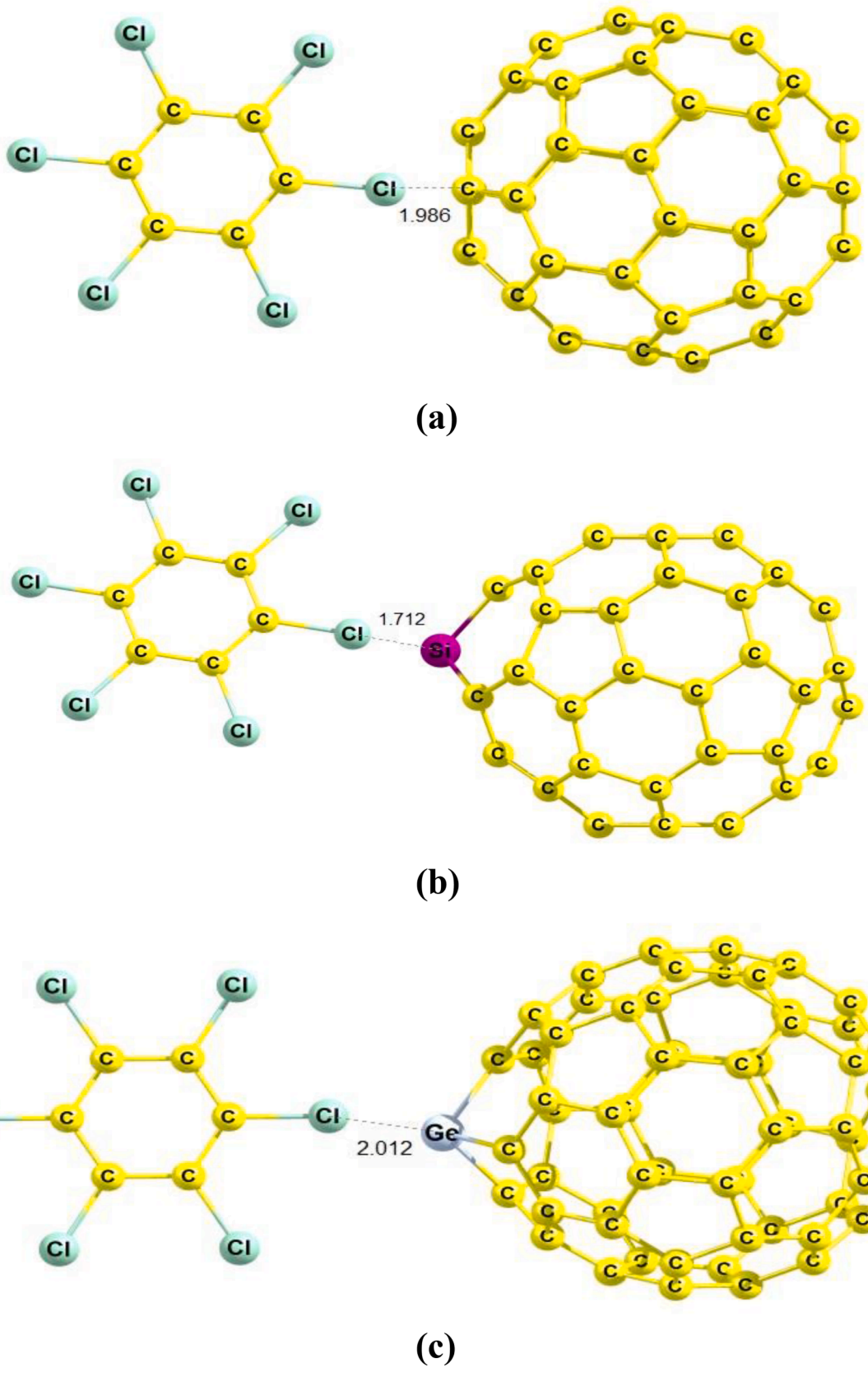


**Fig. 4.** The most stable form of (a) HCB/$C_{60}$, (b) HCB/$C_{59}$Si, and (c) HCB/$C_{59}$Ge, optimized using the B3LYP-D3 functional and 6-311G(d) basis set, showing distance of adsorption in Å.

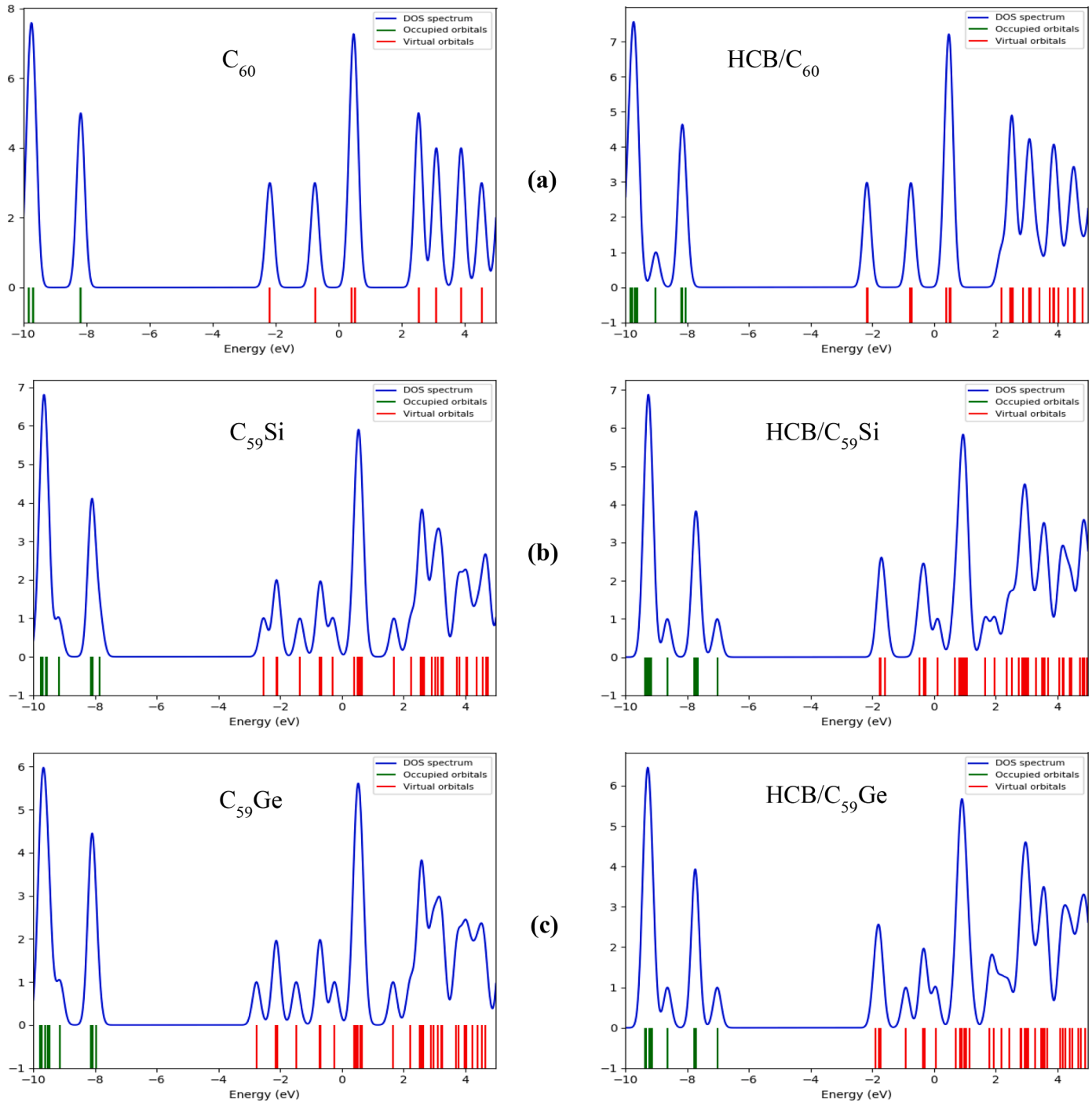


**Fig. 5.** Plot for density of state: (a) $C_{60}$ and HCB/$C_{60}$, (b) $C_{59}Si$ and HCB/$C_{59}Si$, and (c) $C_{59}Ge$ and HCB/$C_{59}Ge$.

**Table 1**
Calculated values for HOMO, LUMO, Energy gap and quantum descriptors for isolated and adsorbed surface evaluated at the B3LYP-D3/6-311G (d) level of theory.

| Systems | $e_{H\ eV}$ | $e_{L\ eV}$ | *EG eV* | $m\ eV^{-1}$ | $h\ eV^{-1}$ | $w\ eV^{-1}$ |
|---|---|---|---|---|---|---|
| **$C_{60}$** | −8.176 | −2.179 | 5.996 | −5.177 | 2.998 | 40.183 |
| **$C_{59}Si$** | −7.848 | −2.540 | 5.309 | −5.194 | 2.654 | 35.805 |
| **$C_{59}Ge$** | −7.954 | −2.766 | 5.188 | −5.360 | 2.594 | 37.266 |
| **HCB/$C_{60}$** | −7.316 | −2.334 | 4.983 | −4.825 | 2.491 | 29.002 |
| **HCB/$C_{59}Si$** | −6.653 | −2.624 | 4.029 | −4.638 | 2.014 | 21.668 |
| **HCB/$C_{59}Ge$** | −7.003 | −2.576 | 4.427 | −4.789 | 2.214 | 25.386 |

**Table 2**
Energy of adsorption ($E_{ads}$) for $C_{60}$, $C_{59}Si$, and $C_{59}Ge$ with Hexachlorobenzene molecule using different functionals.

| Systems | PBE0 eV | B3LYP-D3 eV | M06-2X eV | ωB97XD eV |
|---|---|---|---|---|
| **HCB/C60** | −0.201 | −0.354 | −0.311 | −0.401 |
| **HCB/C59Si** | −0.372 | −0.533 | −0.541 | −0.576 |
| **HCB/C59Ge** | −0.569 | −1.010 | −0.889 | −0.918 |

B3LYP-D3 functionals are due to the long-range dispersion correction which is excellent in predicting interactions [32]. Among the four different functionals, the values obtained

from the B3LYP-D3/6-311G (d) model showed the highest stability, based on the absolute value of the highest absorption energy. Doped surface germanium produced the highest adsorption energy of −1.010 eV. We can conclude that HCB is best adsorbed in $C_{59}Ge$.

### 3.4. Natural bond orbital (NBO) analysis

In this study, natural bond orbitals (NBO) were utilized to study the intermolecular and intramolecular interaction of the donor and acceptor orbitals. NBO provides insights concerning hybridization, charge transfer, and delocalization of electrons [31].. The second-order perturbation energy is used to understand the interaction between molecular orbitals. The stability of a chemical bond can be determined by the bond order [29]. It is also a bond strength index that is commonly utilized in the valence bond theory. NBO was utilized to analyze bond orders, and the methodologies used were Mulliken, Mayer bond order, and Wiberg bond index (WBI) [33]. Mayer bond order is an extension of the Wiberg bond that is useful in bonding analysis. In bonding analysis, ring size and electron count are critical. The bond order of Mulliken and Mayer is related to the Wiberg bond index, which aids in understanding bond strength and overlap between two atoms [33]. From results in Table 3, Weak and electrostatic type of interactions is described by WBI values less than 0.5 whereas values for WBI greater than 0.5 suggest strong interactions. WBI value for Interaction between gas molecule and surfaces in study are observed to be less than 0.5; $C_{60}$ (0.200 *e*), $C_{59}Si$ (0.221 *e*) and $C_{59}Ge$ (0.413 *e*) respectively which indicates weak electrostatic interaction [34]. We can infer that $C_{59}Si$ and $C_{59}Ge$ can serve as adsorbent for Hexachlorobenzene gas.

### 3.5. Quantum theory of atom in molecules (QTAIM) analysis

Many studies concerning critical points and bond pathways in van der Waals and weak interactions have been performed, because bond paths exist, the van der Waals interactions have been classified as directional bonded interactions [34]. For topological analysis, Bader's theory for the quantum theory of atoms in molecules (QTAIM) is employed. This idea has aided in the discovery of inter-atomic and intra-atomic interactions [18]. QTAIM analysis aids in understanding the nature and structure of bond [35]. The electron density and gradient paths indicate the structure of a molecule. Bond critical points (BCP) shows physical relationship between atoms and how molecules interact, and the presence of BCP between gas molecules and nanocages indicates interaction. BCP points indicating an interaction between adsorbing surface and gas molecule is presented in Fig. 6. The density of all electrons $\rho(\mathbf{r})$, describes the probability of finding an electron at a particular distance from the nucleus [36]. Laplacian electron density $\nabla^2\rho(\mathbf{r})$, the amount of electrons in an atom or molecule that can be measured by taking the second partial derivative of the total electron density. In quantum chemistry calculations, it is frequently used to compute the electrostatic potential, electron-electron repulsion energy, and electron-nuclear attraction energy [37]. Lagrangian kinetic energy G(r), is used to analyze the behavior of an electron in a system, this gives information about the nature of atom-atom bonding, and provide a molecular structure for the molecule [38]. Also, potential energy density V(r), and energy density H(r), the potential energy density V(r) is used to analyze the bonding properties of atoms in molecules. It provides a molecular structure for the molecule and helps inform about the nature of the bonding between the atom whereas the energy density is used to determine the total energy stored in a region of space, and when combined with the potential energy density, it can be used to calculate the total potential energy of a particle or system [36,38]. And the bond elliptical index ($\varepsilon$), describe the stability of bonded atom in a system [39]. The bond strength is determined by $\rho(\mathbf{r})$ in BCP. Covalent interactions are defined as energy density H(r) > 0; H(r)/(r) > 0; and G(r) /|V|(r) > 1, A stable repulsive or attractive force between atoms is described as covalent interactions. Non-covalent interactions are defined as H(r) > 0; H(r)/(r) > 0; and G(r) /|V|(r) > 1 [20]. Non-covalent interactions between molecules, rather than between atoms in the same molecule, are known as intermolecular forces. Non-covalent interactions can be classified into electrostatic, hydrophobic and van der waals. Also, large values for Density of all electrons $\rho(\mathbf{r})$ indicates concentration of charge between nuclei. The positive values of the Laplacian ($\nabla^2\rho(\mathbf{r}) > 0$) and the low values of $\rho(\mathbf{r})$ indicate a closed shell interaction (hydrogen and van der waals bond) and suggest charge transfer between two nuclei [31]. The virial theorem suggests a relationship between $G(\mathbf{r})$, $V(\mathbf{r})$, and $\nabla^2\rho(\mathbf{r})$.

$$\frac{1}{4}\nabla^2\rho(\mathbf{r}) = 2G(\mathbf{r}) + V(\mathbf{r}) \tag{6}$$

Bond elliptical index ($\varepsilon$), is necessary for detecting stability which is necessary in adsorption studies. Large values for ε indicates structural instability (ε > 1), whereas when ε < 1 we can infer structural stability. ε can be used to refer to the stability of the interactions and is defined as follows [31].

$$\varepsilon = \frac{\lambda_1}{\lambda_2} - 1; \lambda_1 < \lambda_2 < 0; \; and \; \lambda_3 > 0 \tag{7}$$

According to the results in Table 4, HCB/C60 (0.9327) and HCB/C59Ge (0.1879) have positive values for Laplacian electron density $\nabla^2\rho(\mathbf{r})$ indicating non-covalent interaction, whereas HCB/C59Si (−2370) has a negative value, indicating covalent interaction. For C59Si, the G(r)/|V|(r) value is less than 0.5, indicating that it is effective at adsorbing Hexachlorobenzene gas. Because the values of G(r)/|V|(r) are between 0.5 and 1, the interactions of C60 and C59Ge with HCB tend to be strong in van der Waals. These is supported by H(r) and H(r)/(r) results. Interestingly, when $\lambda_2$<0, information about contributions to non−covalent interactions is provided whereas when $\lambda_2$>0 indicates repulsive contributions. The stability of surfaces after adsorption of the investigated gas is depicted by smaller values obtained from ε as visible in Table 4. Values for ε < 1 are observed for studied adsorption and depicts stability of surfaces upon gas adsorption.

### 3.6. Non-covalent interaction (NCI) analysis

The proposed reduced density gradient (RDG), shows the interaction between two molecules and is defined by [40,41]:

$$RDG = \frac{1}{2(3\pi^2)^{\frac{1}{3}}} \frac{|\overline{\Delta\rho}(\mathbf{r})|}{\rho(\mathbf{r})^{\frac{4}{3}}} \tag{8}$$

RDG and sign $\lambda_2$ (r)p(r) are plotted to define specific areas. the sign$\lambda_2(r)\rho(r)$ is placed on the x-axis, and the RDGs are displayed on the vertical axis [31]. A two-dimensionless coordinate plane is used to display the values of these functions. Non-covalent interaction is of critical importance in chemical and biological interactions [42], and also studies weak interactions. The visualization of non-covalent interactions is based on the analysis of the electron densities and their reduced gradients. The density ($\nabla\rho = 0$) indicates interaction between atoms. the scatter plot of RDG and sign$\lambda_2$ in low-RDG region is used to visualize non-covalent interaction. Non-covalent interactions that are said to be strong are found in the sign$\lambda_2(\mathbf{r})\rho(\mathbf{r}) \approx 0$ region, the sign$\lambda_2(\mathbf{r})\rho(\mathbf{r}) < 0$ region indicates relatively weak van der Waals interactions while repulsive forces are defined in the sign$\lambda_2(\mathbf{r})\rho(\mathbf{r}) > 0$ region. NCI plots for isolated and adsorbed nanocage has been done using B3LYP-D3/6-311G

**Table 3**
Values for Mulliken, Mayer, and Wiberg bond index obtained for studied adsorptions.

| Systems | Mulliken *e* | Mayer *e* | Wiberg *e* |
|---|---|---|---|
| **HCB/$C_{60}$** | 0.071 | 0.089 | 0.200 |
| **HCB/$C_{59}$Si** | 0.191 | 0.199 | 0.221 |
| **HCB/$C_{59}$Ge** | 0.234 | 0.330 | 0.413 |

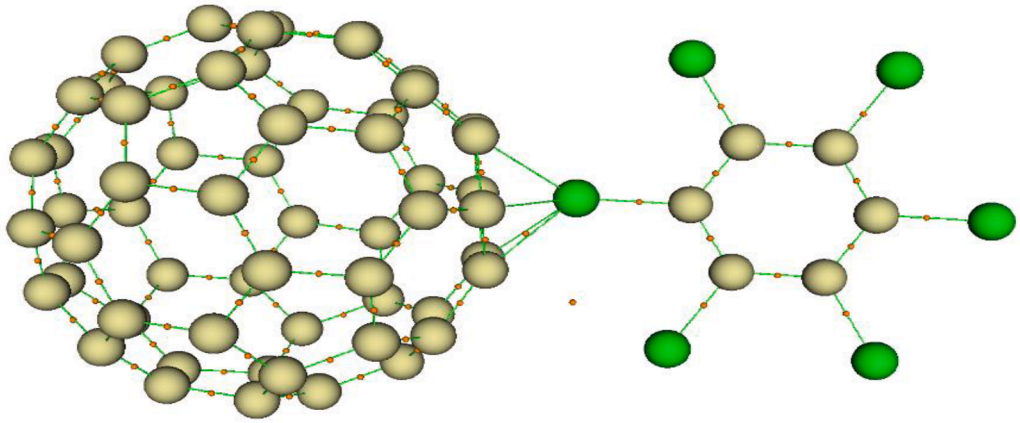

(a)

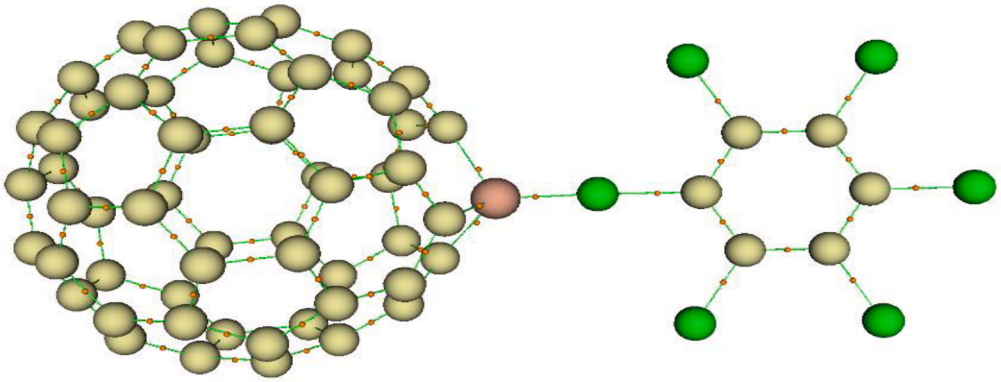

(b)

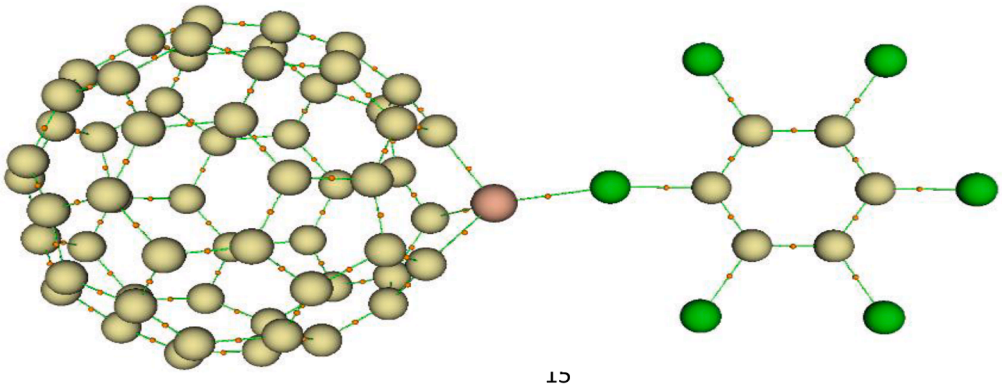

(c)

**Fig. 6.** AIM molecular graphs for studied adsorptions. Orange dots represent the bond critical points (BCPs).

**Table 4**
Topological parameters for studied adsorptions.

| Systems | $r$ | $\bar{N}^2r$ | $G$(r) | $V$(r) | $G$(r)/$V$(r) | $l_1$ | $l_2$ | $l_3$ | $e$ |
|---|---|---|---|---|---|---|---|---|---|
| **HCB/$C_{60}$** | 0.1487 | 0.9327 | 0.2951 | −0.3570 | 0.8266 | −0.2135 | −0.2165 | 1.3627 | 0.0136 |
| **HCB/$C_{59}$Si** | −0.2043 | −0.2370 | 0.0841 | −0.2274 | 0.3697 | −0.2846 | −0.3121 | 0.3598 | 0.0966 |
| **HCB/$C_{59}$Ge** | 0.1184 | 0.1879 | 0.1083 | −0.1695 | 0.6385 | −0.1292 | −0.1281 | 0.4452 | 0.0085 |

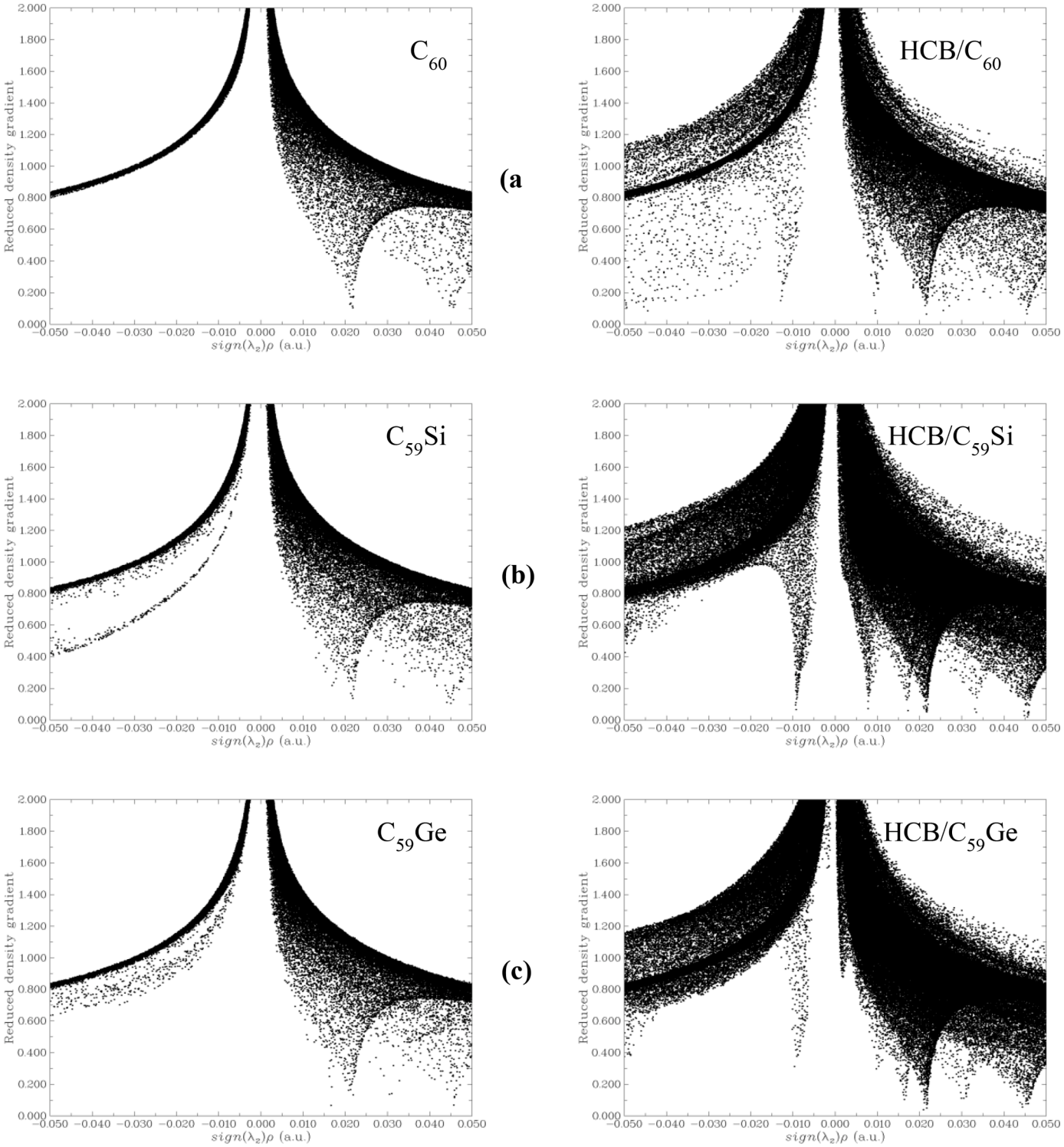


**Fig. 7.** RDG and sign($\lambda_2$)$\rho$(r) plots for Isolated and adsorbed surface.

(d) level of theory and is presented in Fig. 7. The spikes in the −0.010 - 0.010 range show weak van der Waals interactions that are both stabilizing (negative values) and destabilizing (positive values) [39]. The interaction for Ge-doped nanocage has been reported to be non-covalent in previous sections, which agrees with NCI analysis. The absence of dipole-dipole moment is due to the electronegative nature of the element silicon and germanium. NCI analysis is deployed to confirm the accuracy of these results. For $C_{59}Si$ and $C_{59}Ge$ adsorbents, the adsorption intensity is stronger in reference to, $\text{sign}\lambda_2(r)\rho(r) \approx 0$ and $RDG \approx 0.5$. The spikes in the 0.010–0.010 range show weak van der Waals interactions that are both stabilizing (negative values) and destabilizing (positive values).

## 4. Conclusions

In the present investigation, employing the B3LYP-D3, PBE0, ωB97XD, and M06-2X functionals, at the 6-311G(d) basis set, the geometry optimization of the surfaces and complexes were computed. The outcomes of these calculations were impacted by the dispersion correlation in these functionals. Adsorption energies obtained were high and negative, with the highest being at the ωB97XD functional at −0.401 eV for HCB at C60, while the lowest was seen at PBE0 with −0.201 eV. For HCB/C59Si, similar energy ranges were seen with B3LYP-D3 (−0.533 eV) and M06-2X (−0.541 eV) functional. For HCB/C59Ge, ωB97XD yielded the highest adsorption energy at −0.918 eV. The order of high adsorption energies for employed functionals followed a trend of; ωB97XD>M06-2X>B3LYP-D3>PBE0. Our results showed that C59Si and C59Ge were better gas molecule adsorbers with higher intensity. Weak and electrostatic interactions were observed with WBI values less than 0.5. The conductivity of investigated surfaces had similar energy gaps; 5.996, 5.309, and 5.188 eV respectively, indicating the suitability of adsorbent materials for this study QTAIM and NCI analysis revealed non-covalent interactions for C60 and C59Ge nanocages, as well as covalent interactions for C59Si. Overall, these findings showed that Hexachlorobenzene gas can be adsorbed by the nanocages studied, with favorable interactions between the gas and the adsorbent.

## Declarations

*Availability of data and material*

All data are contained within the manuscript.

## Funding

This work was not funded by any agency.

## CRediT authorship contribution statement

**Mohsen D. Mohammadi:** Project administration, Conceptualization, Data curation, Formal analysis. **Hewa Y. Abdullah:** Investigation, Methodology. **Hitler Louis:** Project administration, Resources, Software. **Emmanuel E. Etim:** Writing – original draft. **Henry O. Edet:** Writing – review & editing. **Obinna C. Godfrey:** Visualization, Validation.

## Declaration of Competing Interest

On behalf of the co-authors, of the manuscript titled "Hexachlorobenzene (HCB) adsorption onto the surfaces of $C_{60}$, $C_{59}Si$, and $C_{59}Ge$: Insight from DFT, QTAIM, and NCI" we declare no Conflict of any sort

I can confirm that authors do not have conflicting interest.

## Data availability

Data will be made available on request.

## Acknowledgements

The authors would like to thank the Solid-State Theory Group at the Physics Department at the Universita'degli Studi di Milano-Italy for providing computational facilities and expresse sincere thanks to Prof. Chérif F. Matta, Mount Saint Vincent University, Canada for encouragement and helpful suggestions during this research work.

## References

[1] J.L. Barber, A.J. Sweetman, D. Van Wijk, K.C. Jones, Hexachlorobenzene in the global environment: emissions, levels, distribution, trends and processes, Sci. Total Environ. 349 (1–3) (2005) 1–44.
[2] J. To-Figueras, C. Barrot, M. Rodamilans, J. Gomez-Catalan, M. Torra, M. Brunet, J. Corbella, Accumulation of hexachlorobenzene in humans: a long standing risk, Hum. Exp. Toxicol. 14 (1) (1995) 20–23.
[3] J.J. Zhang, B. Wen, X.Q. Shan, S. Zhang, S.U. Khan, Temporal change in the distribution patterns of hexachlorobenzene and dichlorodiphenyltrichloroethane among various soil organic matter fractions, Environ. Pollut. 150 (2) (2007) 234–242.
[4] S. Deng, N. Feng, S. Kang, J. Zhu, B. Yu, J. Chen, X. Xie, Mechanochemical formation of chlorinated phenoxy radicals and their roles in the remediation of hexachlorobenzene contaminated soil, J. Hazard. Mater. 352 (2018) 172–181.
[5] H. Zhang, L. Jiang, X. Zhou, T. Zeng, Z. He, X. Huang, S. Song, Determination of hexachlorobutadiene, pentachlorobenzene, and hexachlorobenzene in waste incineration fly ash using ultrasonic extraction followed by column cleanup and GC–MS analysis, Anal. Bioanal. Chem. 410 (7) (2018) 1893–1902.
[6] R.E. Bailey, Global hexachlorobenzene emissions, Chemosphere 43 (2) (2001) 167–182.
[7] J. Wan, L. Chai, X. Lu, Y. Lin, S. Zhang, Remediation of hexachlorobenzene contaminated soils by rhamnolipid enhanced soil washing coupled with activated carbon selective adsorption, J. Hazard. Mater. 189 (1–2) (2011) 458–464.
[8] P. Carsky, M. Urban, Ab Initio Calculations: Methods and Applications in Chemistry, Springer Science & Business Media, 2012 (Vol. 16).
[9] A.A. Ahmed, P. Leinweber, O. Kuehn, A computational study of hexachlorobenzene-soil organic matter-interactions, J. Theor. Comput. Chem. 13 (02) (2014), 1450009.
[10] M. Wagner, K.Y.A. Lin, W.D. Oh, G. Lisak, Metal-organic frameworks for pesticidal persistent organic pollutants detection and adsorption–a mini review, J. Hazard. Mater. 413 (2021), 125325.
[11] C. Cha, S.R. Shin, N. Annabi, M.R. Dokmeci, A. Khademhosseini, Carbon-based nanomaterials: multifunctional materials for biomedical engineering, ACS Nano 7 (4) (2013) 2891–2897.
[12] J. Toulouse, C. Adamo, A new hybrid functional including a meta-GGA approach, Chem. Phys. Lett. 362 (1–2) (2002) 72–78.
[13] V. Vaissier Welborn, T. Head-Gordon, Computational design of synthetic enzymes, Chem. Rev. 119 (11) (2018) 6613–6630.
[14] P. Ranjan, A. Kumar, T. Chakraborty, Computational investigation of Ge doped au nanoalloy clusters: a DFT study, in: IOP Conference Series: Materials Science and Engineering, IOP Publishing, 2016, 012172. Vol. 149, No. 1.
[15] U.R. Fogueri, S. Kozuch, A. Karton, J.M. Martin, The melatonin conformer space: benchmark and assessment of wave function and DFT methods for a paradigmatic biological and pharmacological molecule, J. Phys. Chem. A 117 (10) (2013) 2269–2277.
[16] C.B. Erickson, B.E. Ankenman, S.M. Sanchez, Comparison of Gaussian process modeling software, Eur. J. Oper. Res. 266 (1) (2018) 179–192.
[17] E.D. Glendenning, A.E. Reed, J.E. Carpenter, F. Weinhold, NBO Version 3.1, Gaussian Inc., Pittsburg, PA, USA, 2001.
[18] R.F. Bader, A quantum theory of molecular structure and its applications, Chem. Rev. 91 (5) (1991) 893–928.
[19] T. Lu, F. Chen, Multiwfn: a multifunctional wavefunction analyzer, J. Comput. Chem. 33 (5) (2012) 580–592.
[20] M. Doust Mohammadi, H.Y. Abdullah, Ab initio investigation for the adsorption of acrolein onto the surface of C60, C59Si, and C59Ge: NBO, QTAIM, and NCI analyses, Struct. Chem. 33 (2) (2022) 363–378.
[21] N.M. O'boyle, A.L. Tenderholt, K.M. Langner, Cclib: a library for package-independent computational chemistry algorithms, J. Comput. Chem. 29 (5) (2008) 839–845.
[22] J. Borrill, L. Oliker, J. Shalf, H. Shan, Investigation of leading HPC I/O performance using a scientific-application derived benchmark, in: Proceedings of the 2007 ACM/IEEE Conference on Supercomputing, 2007, pp. 1–12.
[23] F. Weigend, R. Ahlrichs, Balanced basis sets of split valence, triple zeta valence and quadruple zeta valence quality for H to Rn: design and assessment of accuracy, Phys. Chem. Chem. Phys. 7 (18) (2005) 3297–3305.
[24] E. Mangaud, S. Huppert, T. Plé, P. Depondt, S. Bonella, F. Finocchi, The fluctuation–dissipation theorem as a diagnosis and cure for zero-point energy

leakage in quantum thermal bath simulations, J. Chem. Theory Comput. 15 (5) (2019) 2863–2880.
[25] B.Q. Pham, M.S. Gordon, Development of the FMO/RI-MP2 fully analytic gradient using a hybrid-distributed/shared memory programming model, J. Chem. Theory Comput. 16 (2) (2020) 1039–1054.
[26] I.Y. Jeon, H.J. Noh, J.B. Baek, Nitrogen-doped carbon nanomaterials: synthesis, characteristics and applications, Chemistry 15 (15) (2020) 2282–2293.
[27] J. Řezáč, P. Hobza, A halogen-bonding correction for the semiempirical PM6 method, Chem. Phys. Lett. 506 (4–6) (2011) 286–289.
[28] M.D. Mohammadi, H.Y. Abdullah, Vinyl chloride adsorption onto the surface of pristine, Al-, and Ga-doped boron nitride nanotube: a DFT study, Solid State Commun. 337 (2021), 114440.
[29] A.D. Udoikono, H. Louis, E.A. Eno, E.C. Agwamba, T.O. Unimuke, A.T. Igbalagh, A. S. Adeyinka, Reactive azo compounds as a potential chemotherapy drugs in the treatment of malignant glioblastoma (GBM): experimental and theoretical studies, J. Photochem. Photobiol. (2022), 100116.
[30] S. Tariq, M. Khalid, A.R. Raza, S.L. Rubab, S.F. de Alcântara Morais, M.U. Khan, A. A.C Braga, Experimental and computational investigations of new indole derivatives: a combined spectroscopic, SC-XRD, DFT/TD-DFT and QTAIM analysis, J. Mol. Struct. 1207 (2020), 127803.
[31] M.D. Mohammadi, H.Y. Abdullah, S. Bhowmick, G. Biskos, Theoretical investigation of X12O12 (X= Be, Mg, and Ca) in sensing CH2N2: a DFT study, Comput. Theor. Chem. 1198 (2021), 113168.
[32] I.C. Lin, U. Rothlisberger, Describing weak interactions of biomolecules with dispersion-corrected density functional theory, Phys. Chem. Chem. Phys. 10 (19) (2008) 2730–2734.
[33] F.S. Patrick-Inezi, W. Emori, H. Louis, C.G. Apebende, E.C. Agwamba, T. O. Unimuke, J.A. Agwupuye, Analeptic activity of 2-Hydroxyl-5-Nitrobenzaldehyde: experimental, DFT studies, and in silico molecular docking approach, Healthc. Anal. 2 (2022), 100030.
[34] N.K. Monteiro, C.L. Firme, Hydrogen–hydrogen bonds in highly branched alkanes and in alkane complexes: a DFT, ab initio, QTAIM, and ELF study, J. Phys. Chem.A 118 (9) (2014) 1730–1740.
[35] E. Nemati-Kande, R. Karimian, V. Goodarzi, E. Ghazizadeh, Feasibility of pristine, Al-doped and Ga-doped Boron Nitride nanotubes for detecting SF4 gas: a DFT, NBO and QTAIM investigation, Appl. Surf. Sci. 510 (2020), 145490.
[36] H.O. Edet, H. Louis, T.E. Gber, P.S. Idante, T.C. Egemonye, P.B. Ashishie, A. S. Adeyinka, Heteroatoms (B, N, S) doped quantum dots as potential drug delivery system for isoniazid drug: insight from DFT, NCI, and QTAIM, Heliyon (2022) e12599.
[37] G.J. Ogunwale, H. Louis, T.O. Unimuke, G.E. Mathias, A.E. Owen, H.O. Edet, M. Doust Mohammadi, Interaction of 5-fluorouracil on the surfaces of pristine and functionalized Ca12O12 nanocages: an intuition from DFT, ACS Omega (2023).
[38] L. Hitler, J.F. Eze, A.D. Nwagu, H.O. Edet, T.O. Unimuke, E.A. Eno, A.S. Adeyinka, Computational study of the interaction of C12P12 and C12N12 nanocages with alendronate drug molecule, ChemistrySelect 8 (1) (2023), e202203607.
[39] I.K. Petrushenko, K.B. Petrushenko, Physical adsorption of hydrogen molecules on single-walled carbon nanotubes and carbon-boron-nitrogen heteronanotubes: a comparative DFT study, Vacuum 167 (2019) 280–286.
[40] Z. Zhang, J. Xiao, X.J. Chen, S. Yu, L. Yu, R. Si, D. Deng, Reaction mechanisms of well-defined metal–N4 sites in electrocatalytic CO2 reduction, Angew. Chem. Int. Ed. 57 (50) (2018) 16339–16342.
[41] J. Contreras-García, E.R. Johnson, S. Keinan, R. Chaudret, J.P. Piquemal, D. N. Beratan, W. Yang, NCIPLOT: a program for plotting noncovalent interaction regions, J. Chem. Theory Comput. 7 (3) (2011) 625–632.
[42] R.A. Boto, J. Contreras-García, J. Tierny, J.P. Piquemal, Interpretation of the reduced density gradient, Mol. Phys. 114 (7–8) (2016) 1406–1414.